Instrument Science Report WFC3 2019-03

Time-dependent WFC3/IR Bad Pixel Tables

Ben Sunnquist, Gabriel Brammer & Sylvia Baggett

May 1, 2019

Abstract

We generate a collection of time-dependent WFC3/IR bad pixel tables in order to reflect the observed behavior changes of ∼3.5% of the detector pixels since launch. These new tables also incorporate an additional six years of data acquired since the previous bad pixel table update as well as utilize enhanced bad pixel detection methods. We identify and flag bad-in-zeroth-read, dead, hot and unstable pixels on a cycle-by-cycle basis as well as the IR blobs as they appear on the instrument. We find no long-term trends in the number or locations of the bad-in-zeroth-read and dead pixels; however, we observe a linear increase of ∼200 hot pixels per cycle and find that the number of unstable pixels can change by up to ∼4000 pixels per cycle. These new bad pixel tables have been delivered and incorporated into the calwf3 pipeline along with the new accompanying time-dependent WFC3/IR superdarks (Sunnquist et al., 2019). For drizzled data products, a new AstroDrizzle parameter table should be used together with these new reference files in order to recover the stable hot pixels (Mack & Bajaj, 2019).

1 Introduction

While certain WFC3/IR detector characteristics, such as the overall dark current level (Sunnquist et al., 2017) and pixel-to-pixel flat field variations (Ryan Jr. & Baggett, 2015), have remained stable since launch, we find that over 35,000 individual detector pixels (∼3.5% of the detector) have changed their behaviors over this same time period. These behavior changes include a pixel regaining a stable state after years of instability, jumping between

multiple stable dark current levels, becoming hot after exhibiting a normal dark current for years and many other such kinds of behavior patterns (see Figures 1 and 2 or Figure 20 in the Appendix for some examples). Because the previous bad pixel searches (Hilbert, 2012; Dulude et al., 2014-06) combined all of the dark and flat data together over time, they were insensitive to these changing pixel behaviors. In this report, we generate a collection of time-dependent WFC3/IR bad pixel tables that account for these changes while also incorporating an additional six years of data acquired since the previous WFC3/IR bad pixel analyses.

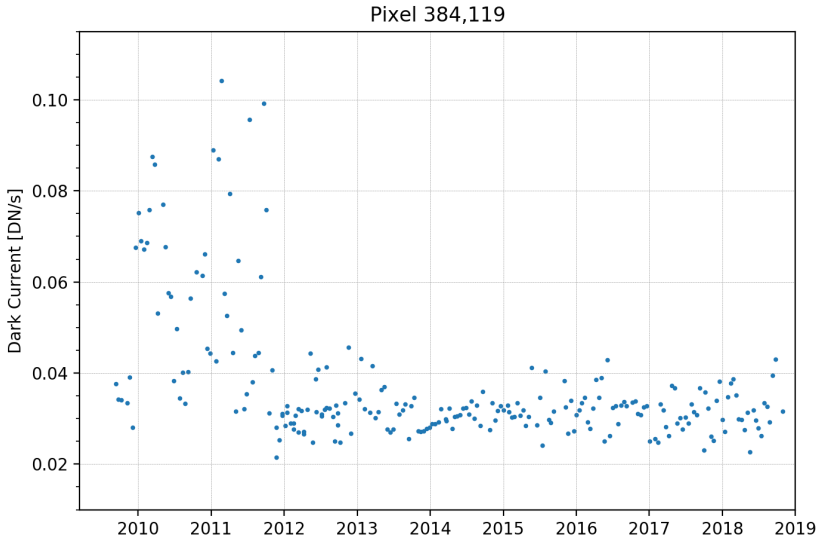

Figure 1: A pixel whose dark current stabilizes after two years of instability.

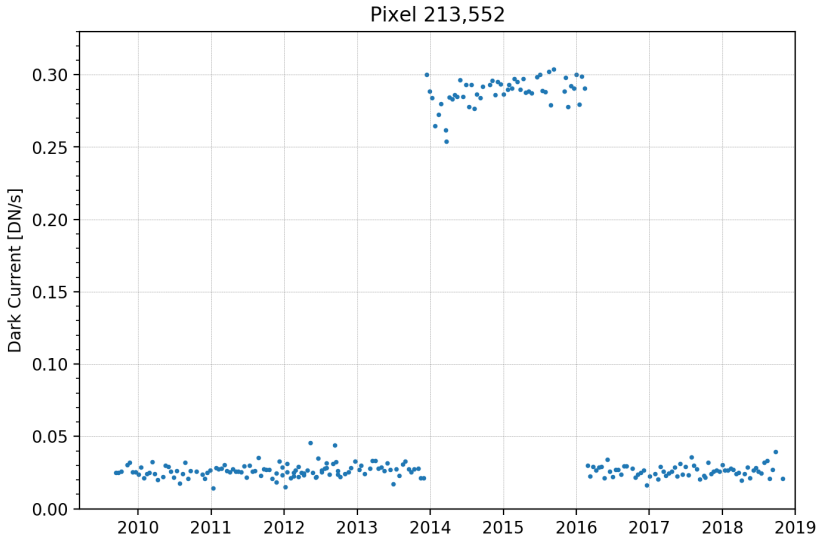

Figure 2: A pixel with a normal dark current that becomes hot for two years before returning to a normal level.

2 Data

We used full-frame dark and flat images from internal WFC3/IR calibration programs to analyze pixel behaviors and determine the bad pixel flags. The darks were observed using a 16-read SPARS200 sample sequence with exposure times of 2803 s. These dark observations have been taken regularly since launch, with each observation spaced ∼2 weeks apart. The flats (images generated by the illumination of the internal tungsten lamp) were observed in the F140W filter with a 14-read RAPID sample sequence and had exposure times of 38 s. These observations did not follow the regular observing cadence of the darks and instead were taken at different intervals throughout each cycle. We calibrated all of these raw files using `calwf3` version 3.4.2 (Jan-19-2018) to obtain the necessary `FLT` and `IMA` images.

For each of these images, we flagged any pixel that was predicted to have persistence levels over 0.001 DN/s (∼ 0.0024 e^-/s, or ∼5% of the median dark rate (Sunnquist et al., 2017)) and discarded them from all of the bad pixel analyses. These persistence predictions came from the persistence products available in the MAST archive (`https://archive.stsci.edu/prepds/persist/search.php`), which provide an estimate of the persistence levels in an image due to IR observations taken up to 16 hours prior to the image. Details on IR persistence and a description of the model can be found in Long et al. (2015). We used the total persistence estimates (i.e. persistence caused by both internal and external sources) for the dark files, but only the external persistence estimates for the flat files; this is due to the flat observations being taken right after other flats with different filters in the calibration programs, which causes the entire image to be affected by persistence. However, since the position of our flats in a visit has remained almost constant from one calibration program to the next, these internal persistence levels are similar between the images. Also, as we'll show in later sections, only flagging the external persistence in these images doesn't noticeably affect our results (i.e. the predicted total persistence levels didn't appear to correlate with the locations of the bad pixels) since the typical total persistence level is only ∼0.2% of the median flat field signal.

Sometimes, the value of a pixel in the dark and flat `FLT` science extensions is zero due to the inability of `calwf3` to perform the up-the-ramp fit; this can be caused for a variety of reasons including low (perhaps even error-prone) saturation values or high up-the-ramp instability. For these pixels, we replaced their `FLT` science array values with the zeroth and reference pixel subtracted final raw read values. We also set the error array values to zero for these pixels which makes it likely that they will be flagged as unstable (see section 4.4). Only about 1500 pixels between the dark and flat images consistently had these zero `FLT` values - most of which were located in the wagon wheel (an area of pixels with lower than normal quantum efficiency clustered in the lower right of the detector) and unbonded pixel areas at the top of the detector.

A summary of all of the data used in the creation of the time-dependent bad pixel tables is shown in Tables 2 and 3 in the Appendix.

3 The Time-dependent Bad Pixel Tables

We generate a collection of time-dependent WFC3/IR bad pixel tables that flag bad-in-zeroth-read, dead, hot and unstable pixels as well as IR blobs and the outermost ring of reference pixels (i.e. the 1-pixel wide border of reference pixels around the detector). We update the bad-in-zeroth-read, dead, hot and unstable pixel flags on a cycle-by-cycle basis and the IR blob flags as needed (see Section 4.5). We set the USEAFTER time in each of these bad pixel tables to the exposure start time of the first full-frame SPARS200 monitoring image in each cycle's dark calibration program (with the exception of the Cycle 17 table, which has an earlier USEAFTER of May 20, 2009 in order to calibrate all of the earliest WFC3/IR data); generally, this USEAFTER time is around late October to early November (Table 1). When new blobs appear, we add the blob to the appropriate bad pixel table and set the USEAFTER in this new table to the appearance time of that blob. For example, if a new blob appeared in March 2013 (part way through Cycle 20), we would generate a new bad pixel table that includes this blob (and all those that appeared before it) with a USEAFTER equal to the appearance time of the new blob. The bad-in-zeroth-read, dead, hot and unstable flags in this table would remain unchanged (i.e. they would remain as those determined using the Cycle 20 calibration data) and the outermost ring of reference pixels would also be flagged (as it always is in every table). See Section 4.5 for more details on how these blobs are identified and flagged.

Table 1: The USEAFTER times for each cycle's bad pixel table. These times determine when a bad pixel table begins to be used in the `calwf3` pipeline.

Cycle	USEAFTER	USEAFTER (MJD)
17	May 20 2009 00:00:00	54971.00000000
18	Nov 01 2010 22:08:59	55501.92290509
19	Nov 02 2011 19:00:44	55867.79217593
20	Nov 01 2012 06:04:35	56232.25318287
21	Oct 21 2013 07:10:39	56586.29906250
22	Oct 24 2014 22:38:39	56954.94350694
23	Nov 03 2015 08:23:25	57329.34959491
24	Oct 08 2016 15:00:50	57669.62557870
25	Oct 02 2017 04:11:11	58028.17443287

4 Bad Pixel Flags

For each cycle, we identify bad-in-zeroth-read, dead, hot and unstable pixels using the darks and flats observed in that cycle's calibration program (see Tables 2 and 3 in the Appendix to see a summary of each cycle's dark and flat calibration data). In addition, we flag the outermost ring of reference pixels and also the IR blobs as they appear in IR images. Many of the bad pixel algorithms we use are based on those that were used to create past WFC3/IR bad pixel tables (Hilbert & Bushouse, 2010; Hilbert, 2012). The main differences are how we identify unstable pixels and incorporate the hot pixel flags - the latter used to be part of the WFC3/IR superdark reference files (Dulude et al., 2014-02) but are now in

the bad pixel tables instead.

4.1 Bad Zeroth Read Pixels

We first identify pixels with abnormal zeroth read signal levels. For each cycle, we create a sigma-clipped mean image of the zeroth read raw signals from that cycle's dark images. Next, we perform a Gaussian fit to each quadrant in this image and flag pixels whose signals are more than 4σ (on the faint end) or 3σ (on the bright end) from the mean (Figure 3). We treat each quadrant separately here as the pixels belonging to each are read out through a different amplifier with a different gain value. This is very similar to the approach outlined in Hilbert (2012), but we've relaxed the threshold on the faint end as these pixels appear to follow the Gaussian fit to lower levels.

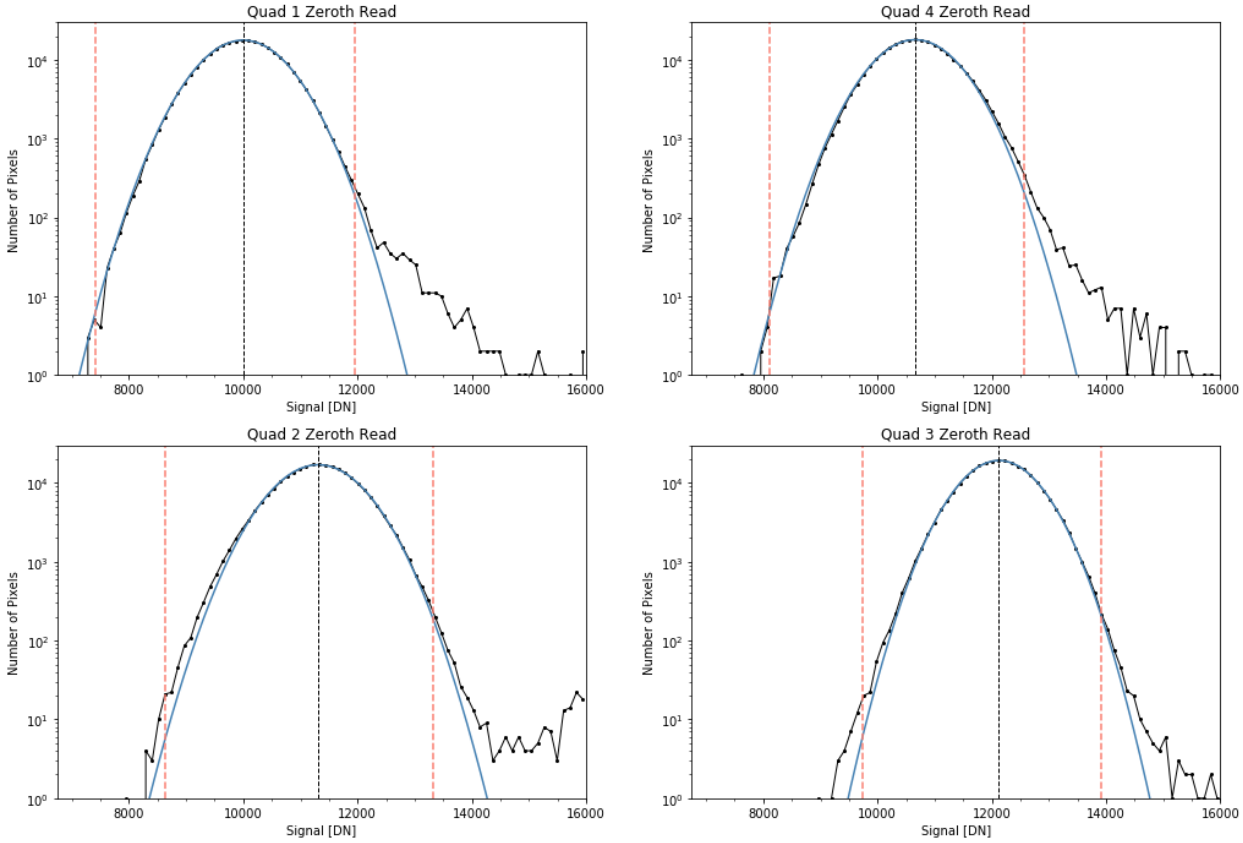

Figure 3: Histograms of the mean zeroth read raw signals in Cycle 25 darks. The orange lines signify the thresholds used for flagging bad zeroth read pixels. Most of the pixels contained in the positive tails of these distributions belong to the unbonded pixel and death star regions, and many of those in the negative tails are located on the border between quadrants 3 and 4. Quadrants of the IR detector are defined as 1-4 counterclockwise from the upper left.

Figure 4 shows an image of all of the bad zeroth read pixels in the Cycle 25 bad pixel table; these are flagged with a DQ value of 8. Many of the bad zeroth read pixels are

contained in the unbonded pixel regions along the top of the detector or in the death star (a circular region of dead and unstable pixels near the bottom left edge of the detector). Figure 5 shows the number of pixels flagged as bad zeroth read pixels in each cycle's bad pixel table. In a typical cycle, we find ∼3100 bad zeroth read pixels (∼0.30% of the detector), and we see no noticeable long-term trends in the number or distribution of this bad pixel population. Because we relaxed one of the thresholds in the bad zeroth read classification, these new time-dependent bad pixel tables flag ∼1800 less bad zeroth read pixels compared to the previous WFC3/IR bad pixel table (Hilbert, 2012).

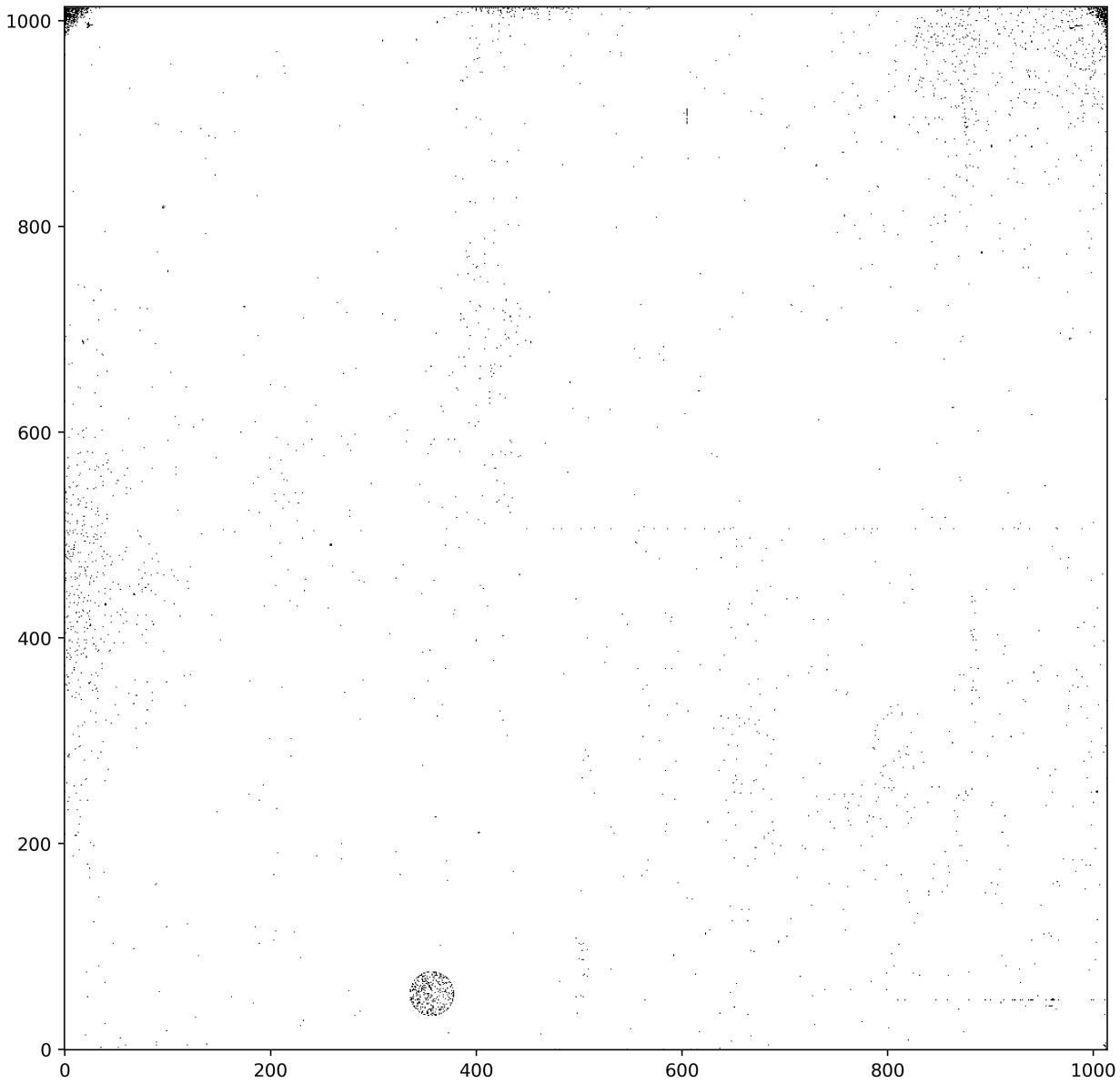

Figure 4: An image showing the pixels flagged as bad zeroth read in the Cycle 25 bad pixel table; these pixels (colored black in this image) are flagged with a DQ value of 8.

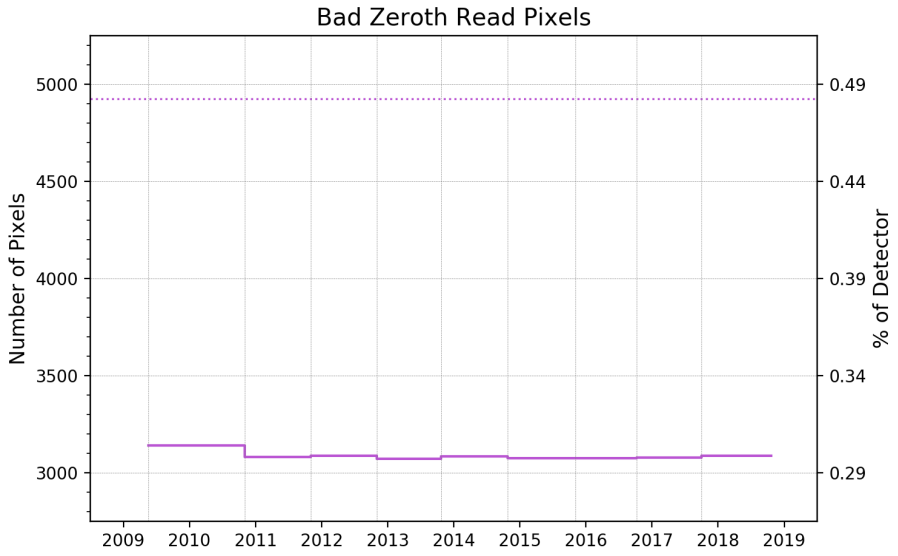

Figure 5: The trends in the number of bad zeroth read pixels as determined from each cycle's bad pixel table. The dotted horizontal line signifies the number of bad zeroth read pixels that were flagged in the previous WFC3/IR bad pixel table (Hilbert, 2012). The vertical lines signify the boundaries of each cycle's bad pixel table (see Table 1).

4.2 Dead Pixels

We next identify pixels that are unresponsive to illumination of the detector. To do this, we create a sigma-clipped mean image of all of the flat `FLT` files for each cycle's calibration program. In each of these mean images, we flag any pixels with zero or negative signal in addition to any pixel whose value is less than 50% of that in the median of a 51x51 pixel box surrounding that pixel. We also include the entirety of the death star in these dead pixel flags. This is again very similar to the method outlined in Hilbert (2012), but we've increased their 30% threshold to 50% to ensure that the unbonded pixels are always flagged as dead in every cycle's bad pixel table.

Figure 6 shows an image of all of the dead pixels in the Cycle 25 bad pixel table; these are flagged with a DQ value of 4. Similar to the bad zeroth read flags, many of these dead pixels are contained in the unbonded pixel regions along the top of the detector or in the death star. Figure 7 shows the number of pixels flagged as dead in each cycle's bad pixel table. In a typical cycle, we find ∼3900 dead pixels (∼0.38% of the detector). Other than the small uptick in the number of dead pixels after the earliest cycle, we see no noticeable long-term trends in the size or location of this bad pixel population. Because we modified one of the thresholds in the dead pixel classification to ensure that the unbonded pixels are always flagged, these new time-dependent bad pixel tables flag ∼560 more dead pixels compared to the previous WFC3/IR bad pixel table (Hilbert, 2012).

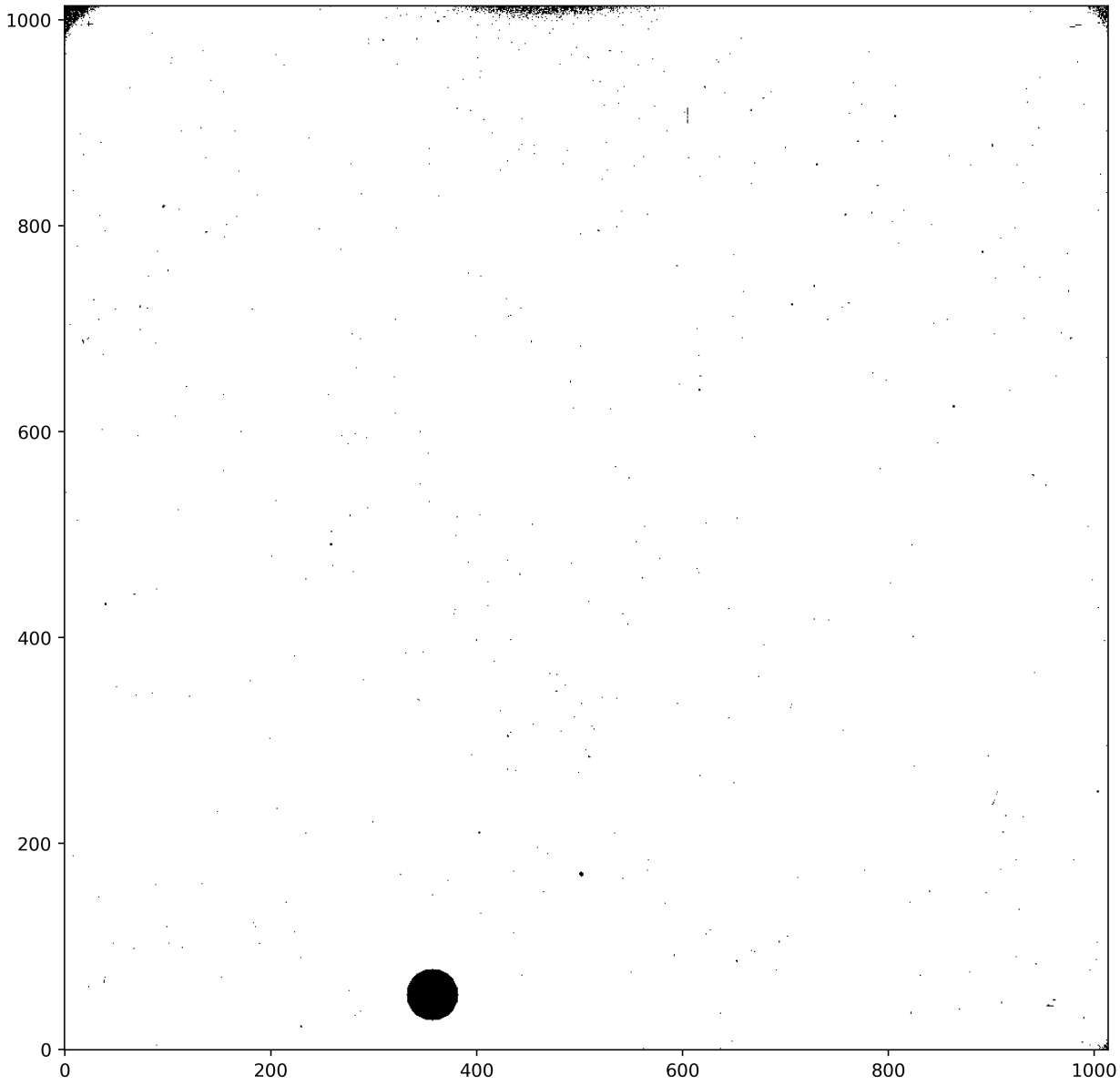

Figure 6: An image showing the pixels flagged as dead in the Cycle 25 bad pixel table; these pixels (colored black in this image) are flagged with a DQ value of 4.

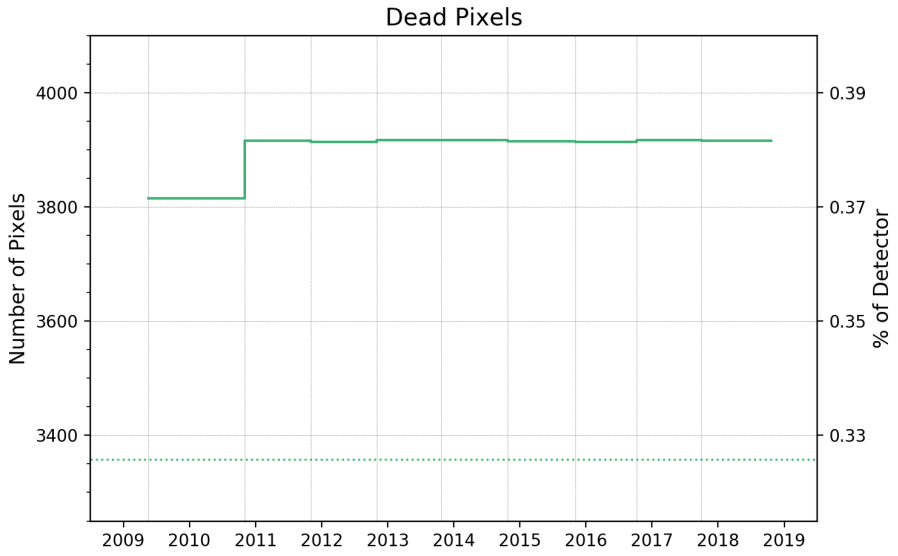

Figure 7: The trends in the number of dead pixels as determined from each cycle's bad pixel table. The dotted horizontal line signifies the number of dead pixels that were flagged in the previous WFC3/IR bad pixel table (Hilbert, 2012). The vertical lines signify the boundaries of each cycle's bad pixel table (see Table 1).

4.3 Hot Pixels

Next, we identify hot pixels, i.e. pixels with abnormally high signals in dark exposures. In the past, these hot pixels were identified during the WFC3/IR superdark generation process and stored in the resulting superdarks' DQ arrays (Dulude et al., 2014-02); however, we've now decided to include these in our time-dependent bad pixel tables and remove them from the superdarks in an effort to keep the various types of bad pixels together in a single file. To identify hot pixels, we create a sigma-clipped mean image of all of the dark `FLT` files for each cycle's calibration program. In each of these images, we then flag any pixels with signals greater than 0.40 e^-/s ($\sim$0.17 DN/s) as hot. This threshold is about eight times greater than the nominal dark current level.

Figure 8 shows an image of all of the hot pixels in the Cycle 25 bad pixel table; these are flagged with a DQ value of 16. Figure 9 shows the number of pixels flagged as hot in each cycle's bad pixel table. We find between $\sim$7100-8500 hot pixels in these bad pixel tables ($\sim$0.69-0.83% of the detector), where the number of hot pixels increases linearly by about 200 per cycle. The number of hot pixels in the earliest bad pixel tables show good agreement with that from the last full-frame SPARS200 superdark that flagged hot pixels (x5g1509ki_drk.fits; Dulude et al., 2014-06). This is not unexpected given the large overlap in the darks used to generate these files (this superdark combined dark files up to mid-2012). Using the unstable flags we will describe in the following section, we find that $\sim$2600-5000 of the identified hot pixels are stable (i.e. their signals vary by about as much as expected from common noise sources such as the read and Poisson noise); the remaining pixels are both hot and unstable.

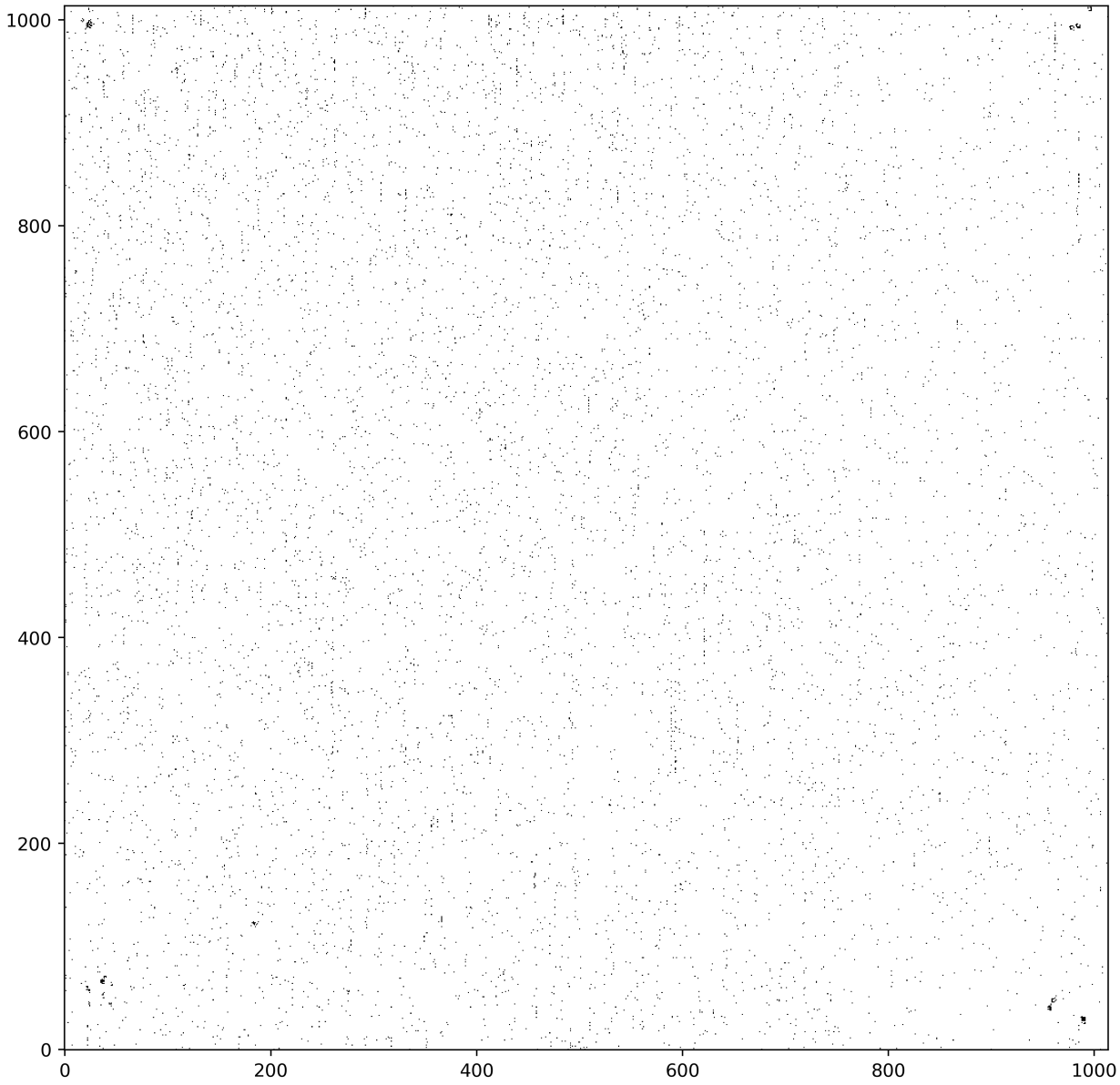

Figure 8: An image showing the pixels flagged as hot (dark current >0.40 e^-/s) in the Cycle 25 bad pixel table; these pixels (colored black in this image) are flagged with a DQ value of 16.

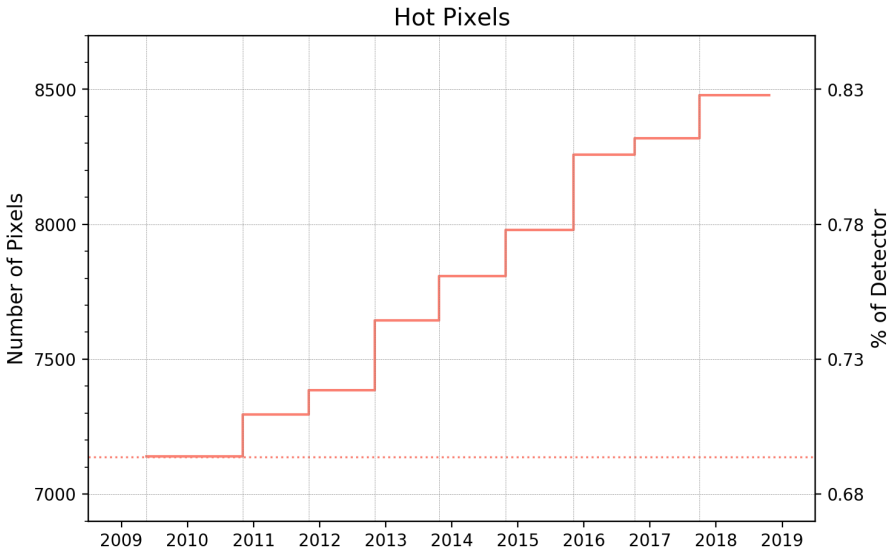

Figure 9: The trends in the number of hot pixels as determined from each cycle's bad pixel table. The dotted horizontal line signifies the number of hot pixels that were flagged in the last WFC3/IR SPARS200 superdark that flagged hot pixels (Dulude et al., 2014-06). The vertical lines signify the boundaries of each cycle's bad pixel table (see Table 1).

4.4 Unstable Pixels

We next flag pixels that show strong variations in their dark or flat signals from exposure-to-exposure. Because pixels can show instability in a variety of ways, we employ multiple methods for catching these unstable pixels. To identify the majority of these pixels, we calculate the ratio of the observed and expected variation of each pixel in the dark and flat `FLT` files from each calibration program and flag any pixels with a ratio greater than 3 (in darks) or 4 (in flats) as unstable, i.e. we flag any pixels varying 3 (or 4) times more than expected in the dark (or flat) observations belonging to each cycle. We refer to this method as the "main unstable method" throughout this section. By using both dark and flat images, we identify pixels that are always unstable as well as those that are only unstable when illuminated. We use the median absolute deviation (MAD) as the observed variation measurement in this ratio (multiplied by 1.483 to make it similar to the standard deviation of a normal distribution) and the median value of the `FLT` error arrays as the expected variation measurement. We opt to use the MAD here as it is more robust to outliers than the standard deviation; we want to avoid flagging pixels that only have a few outliers throughout a cycle since these could be caused by things other than pixel instability (e.g. unmasked persistence, bad up-the-ramp fit due to cosmic ray, etc.). The `FLT` error array values are populated during `calwf3` processing; they are based on the uncertainty of the up-the-ramp fit to the individual samples and, therefore, are influenced by noise sources such as the read and Poisson noise (see Section 3.3.5 of the WFC3 Data Handbook; Gennaro et al., 2018). In Figure 10, we show histograms of these pixel ratios based on Cycle 25 flat and dark images. As expected, the majority of pixels vary by just as much as expected (i.e. they have a ratio of one). Also, it is clear that with our stated thresholds (dotted vertical lines in the plots) we are flagging

pixels well off the normal distribution, so we can be confident that this main unstable method is only flagging truly unstable pixels. Overall, we identify between ∼7900-11000 unstable pixels each cycle using this main unstable method (∼0.77-1.1% of the detector).

As mentioned in Section 2, some pixels always have zero values in their `FLT` science extensions due to the inability of `calwf3` to perform the up-the-ramp fit. For these pixels, we replace their zero `FLT` science values with the zeroth and reference pixel subtracted final raw read values and set their `FLT` error values to zero. By setting the error values this way, we identify these pixels in the main unstable method above as the ratio calculation is infinite (i.e. the denominator is zero). We decide to allow these pixels to be flagged this way as many of the potential reasons for `calwf3` being unable to perform the up-the-ramp fit on these pixels involve abnormal behaviors (e.g. high up-the-ramp instability or error-prone saturation values). We find that ∼1500 of the pixels that are flagged in the main unstable method are the result of this behavior - most of which are located in the wagon wheel and death star regions.

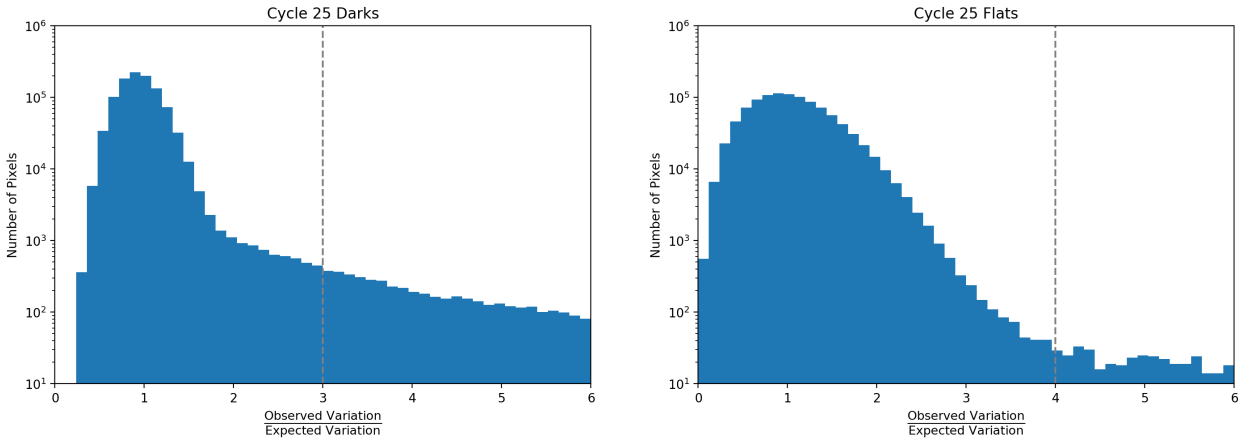

Figure 10: Histograms of the ratios of the observed variation (the median absolute deviations of a pixel's `FLT` science values) to the expected variation (the median of a pixel's `FLT` error values) for each pixel in Cycle 25 darks and flats. The vertical lines signify the thresholds used for flagging unstable pixels.

As a safety precaution, we also flag any pixels whose values in a given cycle have robust standard deviations greater than 0.050 DN/s (0.12 e^-/s) in darks or 30 DN/s (71 e^-/s) in flats. While the main unstable method described above focuses on flagging truly unstable pixels, this safety measure helps satisfy observers who are mainly concerned with the absolute variation of a pixel and not necessarily whether it can be explained by common noise sources or not. We opt to use the robust standard deviation for this safety precaution instead of the MAD (which was used in the main unstable method) because we found that it not only catches those pixels with high variability, but it also catches pixels with other concerning pixel behaviors that are not caught by the MAD (e.g. pixels with many concerning outliers that are otherwise normal or those described in Sections 4.4.1 and 4.4.2). We find that this extra safety measure flags an additional ∼700 pixels in addition to those flagged by the main unstable method.

While the main unstable method provides a robust way to identify general pixel instability, we find that there are certain pixel behaviors that can slip through the flagging when relying only on this method. In the following sections, we explain these pixel behaviors as well as the additional methods we've implemented to identify and flag them. We determine the thresholds for each of these additional methods by careful inspection of the flagged pixel histories after changing each threshold and settle on that threshold which minimizes the number of false and missed pixel flags. Because these additional methods rely on dividing each cycle's data into smaller subgroups, we only implement them using the dark files as typically the number of flat files in a given cycle is insufficient.

4.4.1 Unstable near Cycle Boundaries

Due to the robustness of the main unstable method to outliers, we find that pixels whose dark current turns unstable near a cycle's boundaries may not be flagged as unstable in that cycle. Even though these pixel values are fine for the majority of the cycle, we want to be conservative and flag them within these cycle boundaries since some of the observed instability can be severe (e.g. Figure 11). To catch these pixels, we calculate the MAD (again, multiplied by 1.483 as explained in the main unstable method) of each pixel's values in the 8 earliest and latest darks within each cycle and flag those pixels when either of these values are 4 times greater than the MAD that was calculated for each pixel taking the cycle as a whole. We find that this method identifies an additional ∼500 unstable near cycle boundary pixels not flagged in the main unstable method.

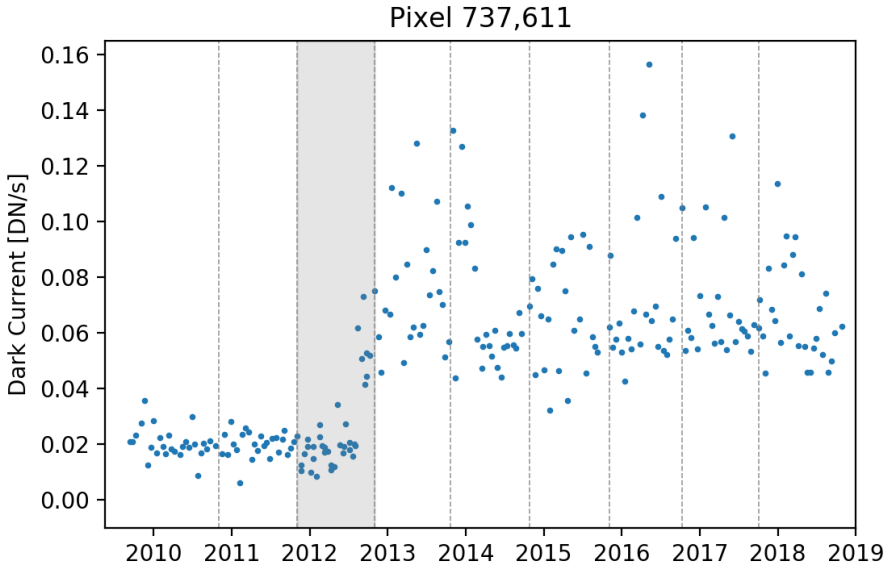

Figure 11: A pixel that turns unstable late in Cycle 19 (shaded) that is caught with the method described in this section. This pixel (and others like it) will be flagged as unstable in the appropriate cycle's bad pixel table.

4.4.2 Signal Jumps

We find that certain pixels jump to different dark current levels within a given cycle. These pixels may be missed by the main unstable algorithm if the jump is small or happens near the cycle boundaries. Figure 12 shows an example of a pixel exhibiting this behavior. To catch these pixels, we calculate the median of each pixel in the 8 earliest and latest dark observations within a given cycle, as well as the median in the 8 observations in the middle of the cycle, and if any of these three values for a given pixel differ by more than 4 times the expected error for that pixel (as determined in the main unstable algorithm), we flag the pixel as unstable. We find that this method flags an additional ∼1500 signal jump pixels not flagged in the main unstable method.

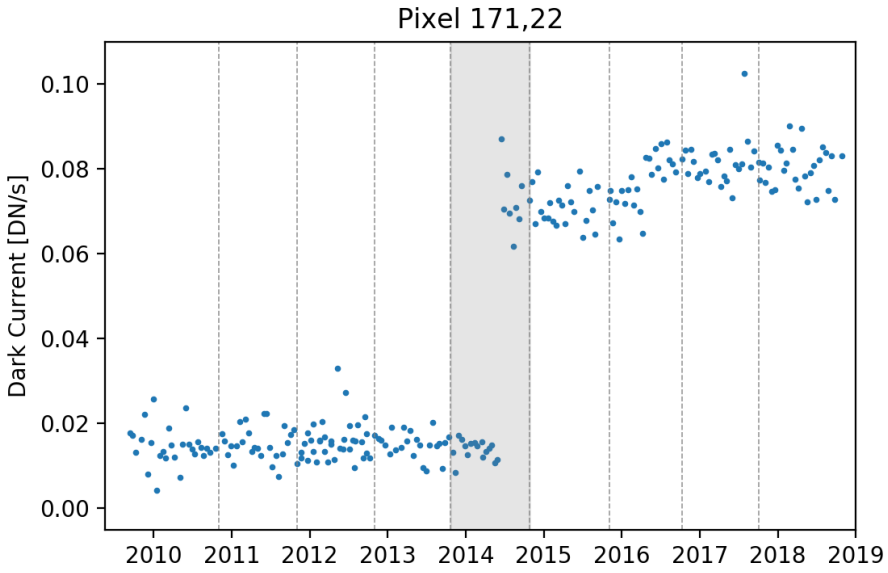

Figure 12: A pixel that steps to a different dark current level in Cycle 21 (shaded) that is caught with the method described in this section. This pixel (and others like it) will be flagged as unstable in the appropriate cycle's bad pixel table

4.4.3 Random Telegraph Noise

We also observe pixels that exhibit random telegraph noise (RTS), where the measured dark current in a pixel randomly oscillates between two different states (see Figure 13 for an example). The main unstable method misses these pixels when the dark current levels of the two states are separated by only a small amount or when the number of observations are not divided equally between the states - resulting in a small MAD. We identify these pixels by calculating the median of the 8 highest and lowest dark current values for each pixel within a given cycle, and we flag any pixel where the absolute difference between these two values is 6 times greater than the expected error for that pixel (determined as in the main unstable algorithm). We find that this method flags an additional ∼2200 RTS pixels not flagged in the main unstable method.

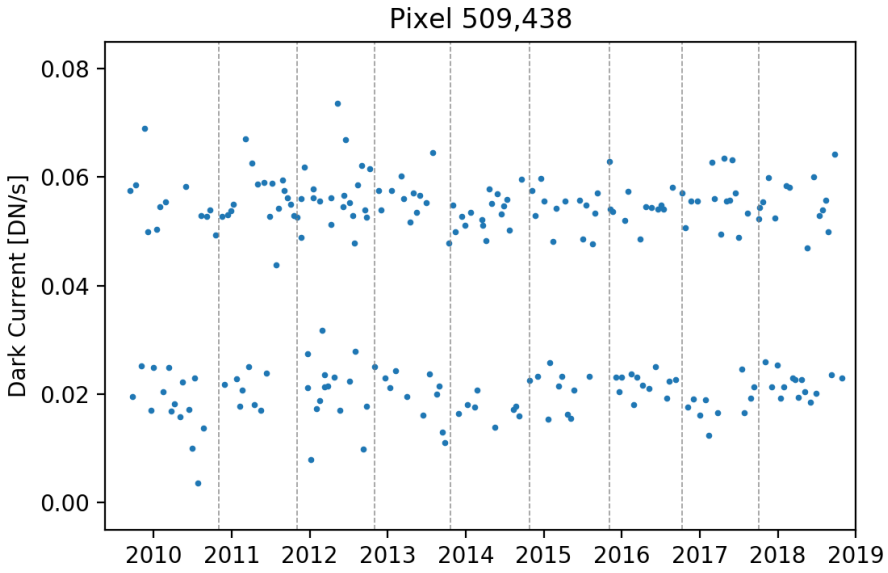

Figure 13: A pixel exhibiting random telegraph noise that is caught using the method described in this section. This pixel (and others like it) will be flagged as unstable in the bad pixel tables.

4.4.4 Cumulative Unstable Flags

After combining all of the unstable methods described in the previous sections, we identify a total of ∼11,000-15,000 unstable pixels in each cycle's bad pixel table (∼1.1-1.5% of the detector) (Figure 15). In Figure 14, we show all of the pixels flagged as unstable in the Cycle 25 bad pixel table; these pixels are flagged with a DQ value of 32. We find that the vast majority of these unstable flags were identified applying the unstable methods to the dark observations and only a small number (<2%) are found solely using the flat observations; this implies that the majority of the identified unstable pixels are unstable whether or not they are illuminated. However, we do acknowledge that the flats were taken less frequently than the darks and also did not have a regular observing cadence - making the time sampling less ideal. In Figure 15, we note a large reduction in the number of unstable pixels on the detector from Cycle 19 to 20. Interestingly, this corresponds to the time (mid-2012) when we stopped warming the IR detector during the UVIS anneals (HST Proposal 12687: WFC3/UVIS Anneal), which may have contributed to the large number of pixels regaining their stability around this time period. Our bad pixel tables flag between ∼1700-5700 fewer pixels than the previous WFC3/IR bad pixel table (Hilbert, 2012); we attribute this to more robust unstable algorithms, better noise control, the incorporation of persistence flagging and the smaller subsets of data used in our cycle-based approach (the previous table combined all data from cycles 17-19, which, as we can see in Figure 15, is the time period where we observe the most instability).

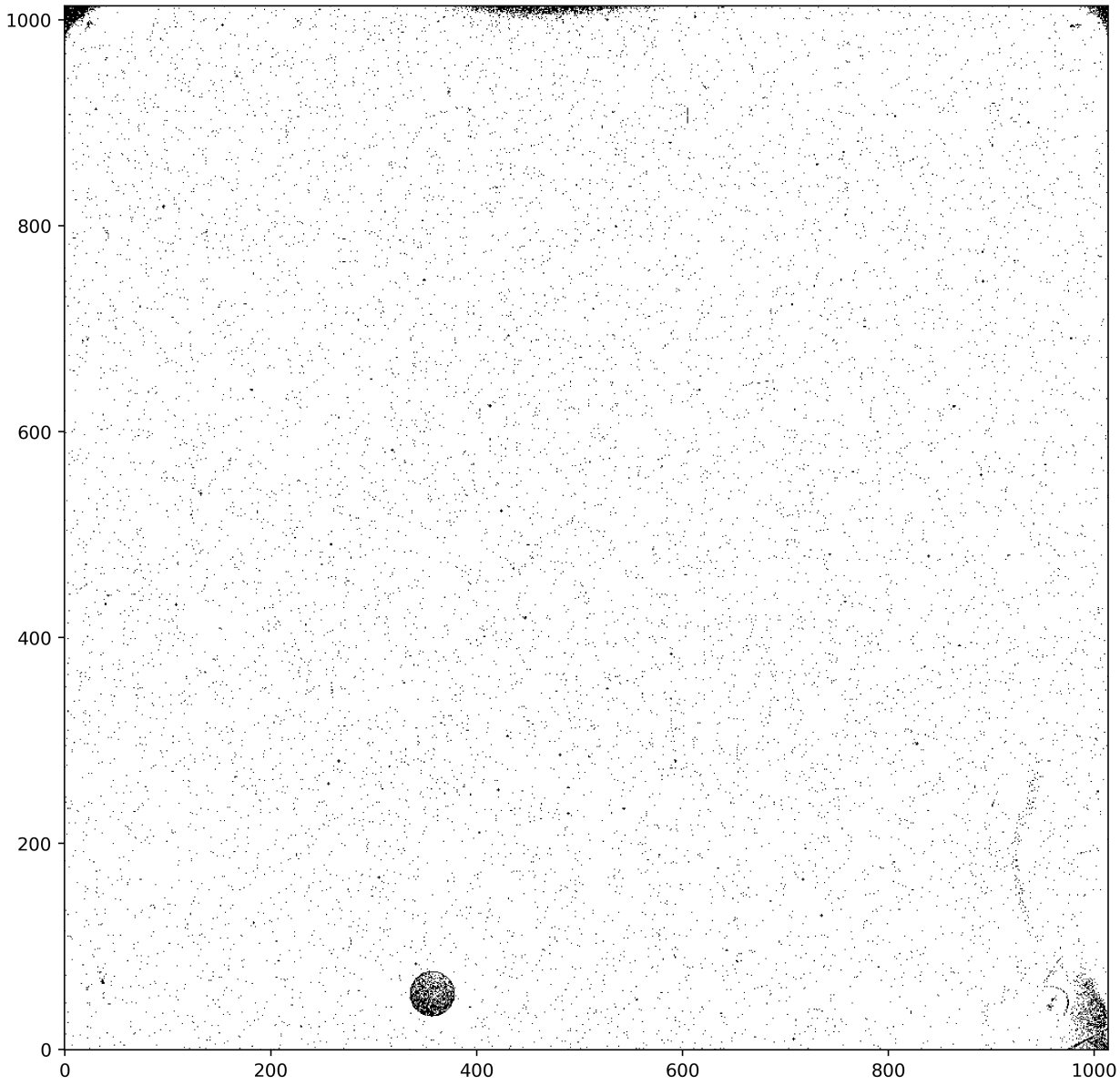

Figure 14: An image showing the pixels flagged as unstable in the Cycle 25 bad pixel table; these pixels (colored black in this image) are flagged with a DQ value of 32.

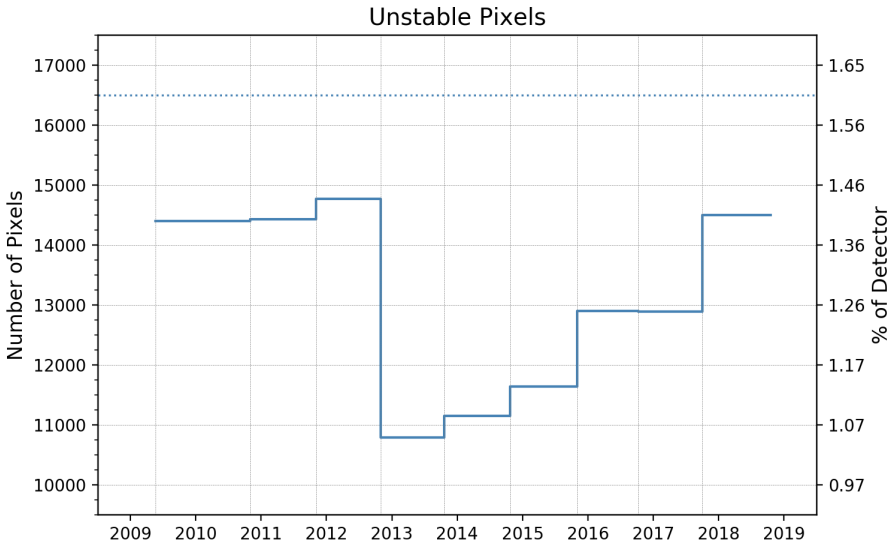

Figure 15: The trends in the number of unstable pixels as determined from each cycle's bad pixel table. The dotted horizontal line signifies the number of unstable pixels that were flagged in the previous WFC3/IR bad pixel table (Hilbert, 2012). The vertical lines signify the boundaries of each cycle's bad pixel table (see Table 1).

4.5 IR Blobs

A growing number of IR blobs (circular regions with decreased light sensitivity) have sporadically appeared in WFC3/IR images since launch. New blob appearances are detected using a dedicated monitoring program that obtains dark-Earth flats ∼weekly; the blobs strongly stand out from the high background levels in these images which allows for the easy identification of any new blobs (Sunnquist, 2018). Once these blobs appear, they remain on the instrument and their positions do not change (Pirzkal & Hilbert, 2012). Whenever strong IR blobs appear, we incorporate them into the relevant cycle's bad pixel table with a DQ flag value of 512 (see McCullough et al. (2014) and Sunnquist (2018) for discussions on how these "strong" blobs are determined). As an example, if a strong blob appears in March 2013 (partway through Cycle 20), we append a mask covering its area to the Cycle 20 bad pixel table and deliver this new bad pixel table with a USEAFTER equal to the appearance time of that blob. The bad-in-zeroth-read, dead, hot and unstable flags remain unchanged in this delivery, as they are only updated once per cycle and, of course, all of the other strong blobs that appeared before this new blob are also included in this delivery. Strong IR blobs affect between ∼4400-11000 pixels (∼0.43-1.1% of the detector; see Figure 17). In Figure 16, we display all blob flags from the final Cycle 25 bad pixel table. We use Table 1 from Sunnquist (2018) as the reference for the blob positions, sizes, strengths and appearance times for our bad pixel tables. Our blob masks are shifted by one pixel down and one pixel to the left compared to the previous bad pixel tables, as we noticed these masks in the old tables were offset from the positions listed in Sunnquist (2018).

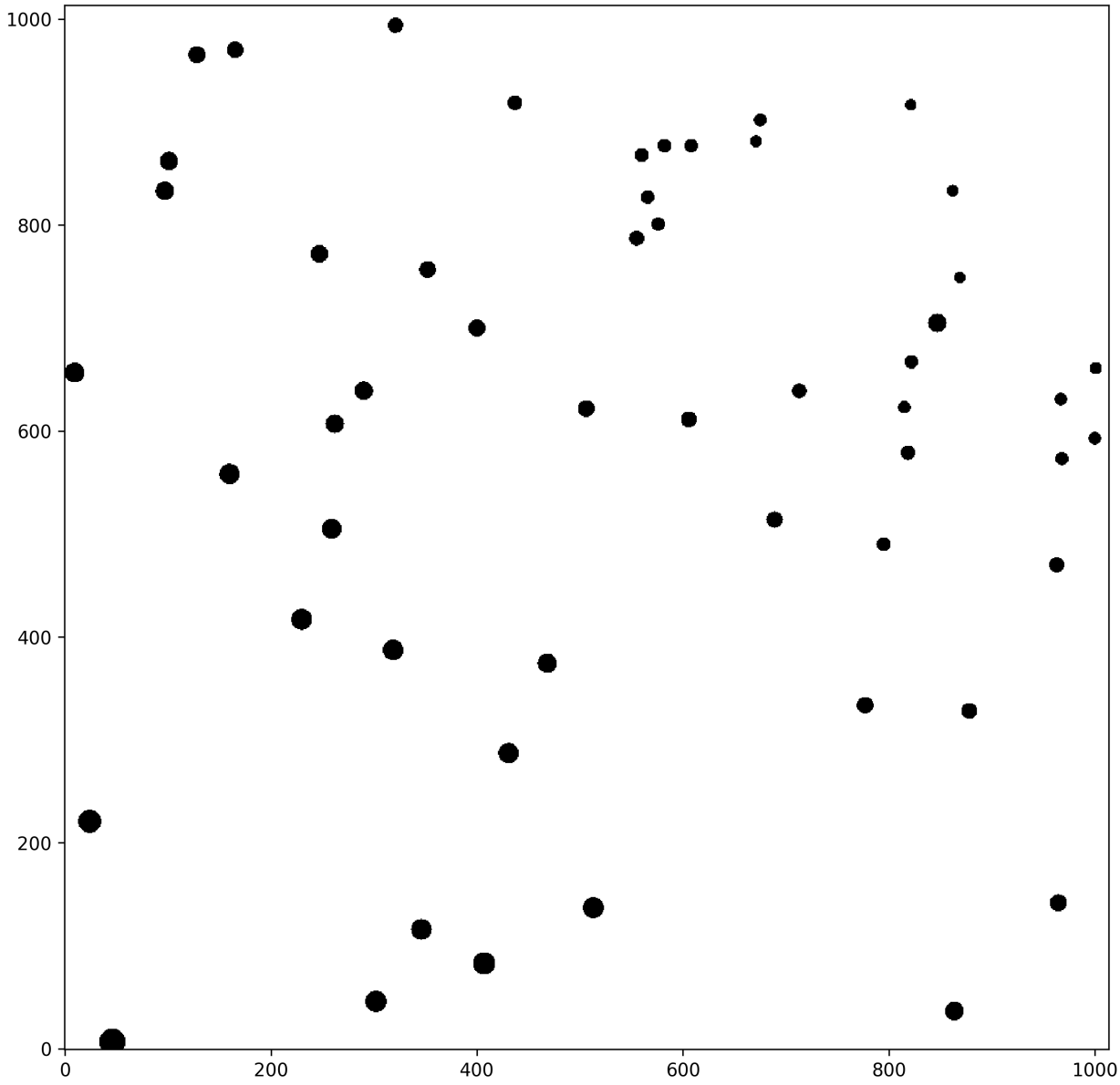

Figure 16: An image showing the pixels flagged as being affected by strong IR blobs in the final Cycle 25 bad pixel table; these pixels (colored black in this image) are flagged with a DQ value of 512.

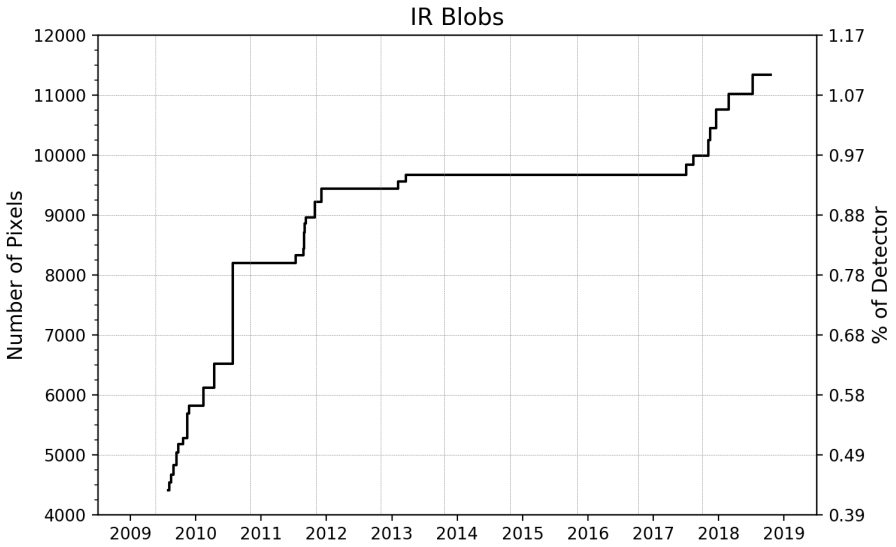

Figure 17: The trends in the number of pixels affected by strong IR blobs. These pixels are flagged with a DQ value of 512 in the bad pixel tables. The vertical lines signify the boundaries of each cycle (see Table 1). The large spike around mid-2010 corresponds to the time when dark-Earth flats replaced sky flats as the images used for new blob detection - allowing for the detection of a large number of previously unknown blobs. Therefore, this spike doesn't actually represent a large number of blobs all appearing at once, but rather is a product of improved detection methods (see Sunnquist, 2018).

4.6 Outboard Reference Pixels

In every bad pixel table, we flag the outermost ring of reference pixels (i.e. the 1-pixel wide border of reference pixels around the detector) with a DQ value of 128. These pixels have a different capacitance and are less numerous than the innermost (inboard) reference pixels, and so they are not used during the bias correction step (BLEVCORR) during `calwf3` processing for all WFC3/IR images (see Section 3.3.3 of the WFC3 Data Handbook; Gennaro et al., 2018).

5 Summary

We generate a collection of time-dependent WFC3/IR bad pixel tables that flag bad-in-zeroth-read, dead, hot and unstable pixels on a cycle-by-cycle basis, along with the outboard reference pixels and strong IR blobs as they appear on the instrument. Figure 18 shows the number of bad-in-zeroth-read, dead, hot and unstable pixels that are flagged in each cycle's bad pixel table, as well as the number of pixels affected by strong IR blobs. Figure 19 shows the location of all the flagged pixels in the final Cycle 25 bad pixel table. We find that the bad-in-zeroth-read and dead pixel populations remain almost constant over time; however, the hot pixel population increases linearly by $\sim$200 pixels per cycle, and the number of unstable pixels can change by up to $\sim$4000 pixels per cycle. Our full collection of time-dependent WFC3/IR bad pixel tables along with the accompanying new time-dependent

WFC3/IR superdarks (Sunnquist et al., 2019) have been delivered and incorporated into the `calwf3` pipeline.

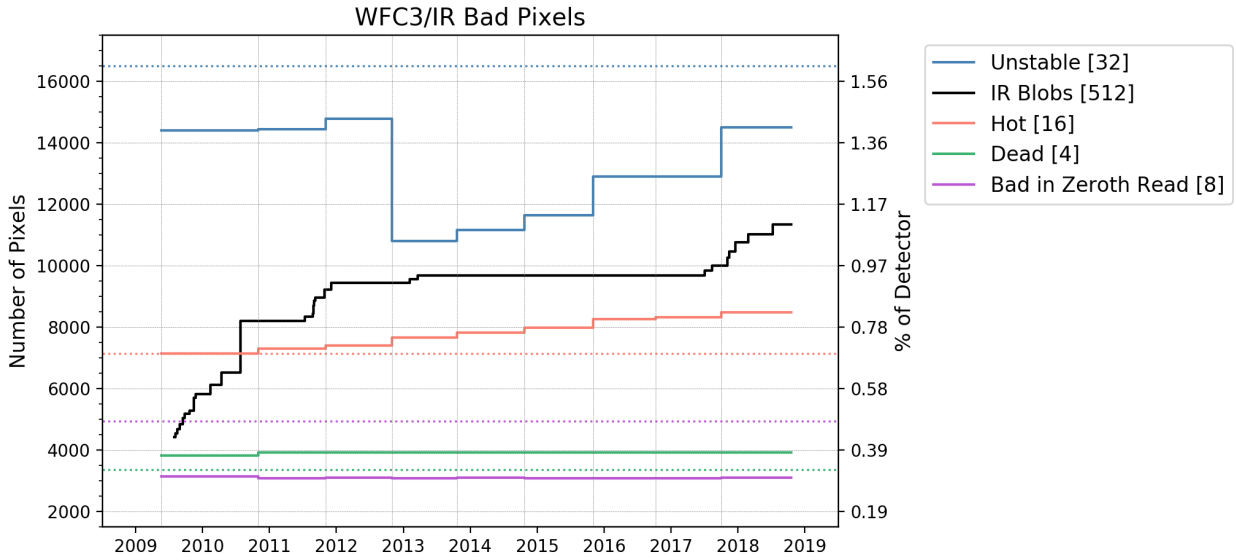

Figure 18: The trends in the various bad pixel populations as determined from each cycle's bad pixel tables. The dotted horizontal lines signify the number of pixels that were flagged the last time these populations were identified (Hilbert, 2012; Dulude et al., 2014-06), and the vertical lines signify the boundaries of each cycle (see Table 1). The numbers in the legend denote the DQ value of the bad pixel type. The bad-in-zeroth-read, dead, hot and unstable pixels have been updated on a cycle-by-cycle basis, while the IR blob flags are superimposed on these as needed - resulting in many cycles having multiple bad pixel tables.

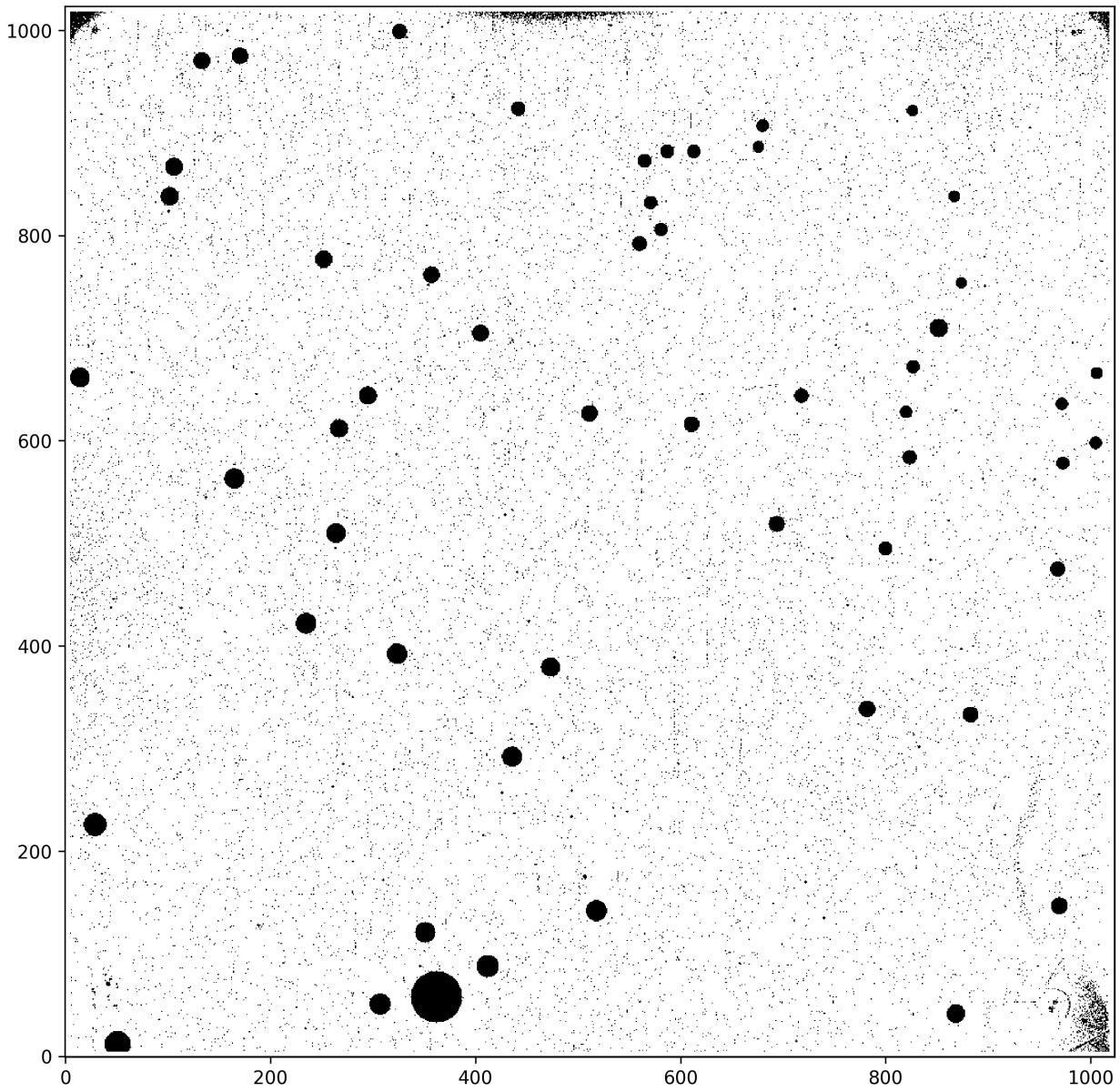

Figure 19: An image showing all flagged pixels (colored black in this image) in the final Cycle 25 bad pixel table.

Recommendations

As of May 2019, the MAST processing pipeline flags stable and unstable hot pixels with different data quality values.

Observers who work directly with the `FLT`/`IMA` files can choose to reclaim the calibrated stable hot pixels by NOT discarding pixels with DQ flag=16. We recommend continuing to treat unstable pixels (DQ flag=32) as bad.

Observers who work with drizzled data (drz files) should note that stable hot pixels (DQ flag=16) are by default reclaimed and treated as good pixels; pixels identified as unstable

(flag=32) continue to be treated as bad. This change has been implemented in the pipeline via an updated AstroDrizzle parameter table (Mack & Bajaj, 2019) which is used in conjunction with the new pipeline darks (Sunnquist et al., 2019) and bad pixel tables (this ISR). The AstroDrizzle parameter table defines the recommended drizzling parameters for each instrument and can be used together with the new calibration reference files in order to recover stable hot pixels in drizzled images. For more information on modifications to the MDRIZTAB settings, please see Mack & Bajaj (2019).

Observers with archival data prior to May 2019 may re-request their data from the MAST portal to have their data automatically reprocessed and redrizzled with the new reference files.

References

Dulude, M.J., Baggett, S., and Hilbert, B., 2014. WFC3 TIR 2014-02. **"WFC3/IR Dark Reference File Generation"**.

Dulude, M.J., Baggett, S., and Hilbert, B., 2014. WFC3 ISR 2014-06. **"New WFC3/IR Dark Calibration Files"**.

Gennaro, M., et al. 2018, "**WFC3 Data Handbook**", Version 4.0, (Baltimore: STScI).

Hilbert, B., and Bushouse, H., 2010. WFC3 ISR 2010-13. **"WFC3/IR Bad Pixel Table: Update Using Cycle 17 Data"**.

Hilbert, B., 2012. WFC3 ISR 2012-10. **"WFC3/IR Cycle 19 Bad Pixel Table Update"**.

Long, K. S., Baggett, S., and MacKenty, J. W., 2015. WFC3 ISR 2015-15. **"Persistence in the WFC3 IR Detector: An Improved Model Incorporating the Effects of Exposure Time"**.

Mack, J., and Bajaj, V., 2019. WFC3 ISR 2019-05. **"Improved Drizzled Data Products for the WFC3/IR Detector"**.

McCullough, P.R., Mack, J., Dulude, M., and Hilbert, B., 2014. WFC3 ISR 2014-21. **"Infrared Blobs: Time-dependent Flags"**.

Pirzkal, N., and Hilbert, B., 2012. WFC3 ISR 2012-15. **"The WFC3 IR "Blobs" Monitoring"**.

Ryan Jr., R. E., and Baggett, S., 2015. WFC3 ISR 2015-11. **"The Internal Flat Fields for WFC3/IR"**.

Sunnquist, B., Baggett, S., Long, K.S., 2017. WFC3 ISR 2017-04. **"An Exploration of WFC3/IR Dark Current Variation"**.

Sunnquist, B., 2018. WFC3 ISR 2018-06. **"WFC3/IR Blob Monitoring"**.

Sunnquist, B., Mckay, M., Baggett, S., 2019. WFC3 ISR 2019-04. **"Time-dependent WFC3/IR Superdarks"**.

Acknowledgments

The authors would like to thank Russell Ryan for the review of this document and for suggesting many useful changes and enhancements. The authors would also like to thank Jennifer Mack, Heather Kurtz, Varun Bajaj & Nor Pirzkal for testing these new reference files and providing useful feedback.

Appendix

Table 2: List of all WFC3/IR darks used in the creation of the time-dependent bad pixel tables. All of these darks were observed using a 16-read SPARS200 sample sequence and have exposure times of 2803 s. See Table 1 for the date range of each cycle.

Proposal ID (Cycle)	Datasets
11929 (17)	ibcu07ykq, ibcu0ldxq, ibcu0yvqq, ibcu1lv1q, ibcu1yi2q, ibcu20djq, ibcu2ldjq, ibcu2ywtq, ibcu33onq, ibcu3lwmq, ibcu3ywvq, ibcu4lfmq, ibcu4ydgq, ibcu59fkq, ibcu5ldbq, ibcu5ydaq, ibcu6lq3q, ibcu6ydsq, ibcu72buq, ibcu7llaq, ibcu7yxnq, ibcu85v8q, ibcu8ldzq, ibcu8yd7q, ibcu98b1q, ibcu9ldzq, ibcuabmaq, ibcub1tyq, ibcubecnq
12349 (18)	iblt0lcxq, iblt15c6q, iblt1bdcq, iblt1rfoq, iblt2hfxq, iblt2xfqq, iblt31bkq, iblt3nbyq, iblt47hbq, iblt4dgwq, iblt4tetq, iblt5jf5q, iblt5zasq, iblt63chq, iblt6plcq, iblt79bgq, iblt7fg2q, iblt7vc7q, iblt8ldzq, iblt95btq, iblt9bf9q, iblt9rbkq, iblta7eas, ibltanamq
12695 (19)	ibvi0bhqq, ibvi0ke8q, ibvi0lefq, ibvi0uhmq, ibvi15feq, ibvi16d1q, ibvi1dudq, ibvi1nfoq, ibvi1wbqq, ibvi1xpkq, ibvi25vdq, ibvi2geqq, ibvi2pjrq, ibvi2qprq, ibvi2zsqq, ibvi34tmq, ibvi35trq, ibvi3ic3q, ibvi3jhwq, ibvi3se5q, ibvi44x7q, ibvi4bfgq, ibvi4ckeq, ibvi4lnrq, ibvi4ubiq, ibvi4vflq, ibvi53cfq, ibvi54ciq, ibvi5ecoq, ibvi63npq, ibvi72a3q, ibvi73s2q, ibvi82faq, ibvi91caq, ibvi92deq
13077 (20)	ic5r05wiq, ic5r06psq, ic5r0fo4q, ic5r0ga4q, ic5r0qg0q, ic5r0rekq, ic5r17nfq, ic5r18c3q, ic5r28mfq, ic5r29kvq, ic5r39mmq, ic5r45azq, ic5r46meq, ic5r55gtq, ic5r56bwq, ic5r67iwq, ic5r68msq, ic5r76afq, ic5r77bzq, ic5r84ovq, ic5r85kqq, ic5r96zrq, ic5r97k8q
13562 (21)	icf901eeq, icf902w5q, icf903acq, icf904i6q,

	icf905crq, icf906giq, icf907xgq, icf908d6q, icf909h7q, icf910hgq, icf911buq, icf912jjq, icf913j1q, icf914ulq, icf915tkq, icf916yiq, icf917wdq, icf918y4q, icf919k8q, icf920xzq, icf921guq, icf922wxq, icf923mrq, icf924dvq
14008 (22)	icqm01qbq, icqm02c1q, icqm03x5q, icqm04ccq, icqm05umq, icqm06tgq, icqm07ttq, icqm08tlq, icqm09bxq, icqm10syq, icqm11roq, icqm12stq, icqm13skq, icqm14qvq, icqm15dhq, icqm16r3q, icqm18d3q, icqm19giq, icqm20ozq, icqm21yoq, icqm22l1q, icqm23r9q, icqm24yfq
14374 (23)	id0c01lqq, id0c02nnq, id0c03zeq, id0c04xkq, id0c05xdq, id0c06bhq, id0c07z5q, id0c08w0q, id0c09cnq, id0c10h3q, id0c11ypq, id0c12bqq, id0c13lbq, id0c14tqq, id0c15baq, id0c16zqq, id0c17ndq, id0c18yoq, id0c19enq, id0c20ydq, id0c21xjq, id0c22y8q, id0c23x6q, id0c24ynq
14537 (24)	idbx01zzq, idbx02nbq, idbx03eeq, idbx04vbq, idbx05irq, idbx06bjq, idbx07rgq, idbx09faq, idbx10ixq, idbx11eaq, idbx12btq, idbx13ybq, idbx14egq, idbx15k1q, idbx16jhq, idbx17duq, idbx18fvq, idbx19crq, idbx20zgq, idbx21wuq, idbx22apq, idbx23ydq, idbx24cxq, idbx25w9q
14986 (25)	idp201byq, idp202jbq, idp203d6q, idp204a4q, idp205ifq, idp206k3q, idp207f7q, idp208mcq, idp209f4q, idp210d3q, idp211giq, idp212eyq, idp213fqq, idp214zrq, idp215gns, idp216fdq, idp217mjq, idp218d8q, idp219atq, idp220hjq, idp221buq, idp222b7q, idp223oxq, idp224ilq, idp225cdq, idp226f3q, idp227i5q, idp229gpq

Table 3: List of all WFC3/IR flats used in the creation of the time-dependent bad pixel tables. All of these flats were taken using the F140W filter. They were observed using a 14-read RAPID sample sequence and have exposure times of 38 s. See Table 1 for the date range of each cycle.

Proposal ID (Cycle)	**Datasets**
11915 (17)	ib9m01bdq, ib9m06j7q, ib9m0anoq, ib9m0erwq, ib9m0fhoq, ib9m11riq, ib9m15diq, ib9m16pjq, ib9m21e5q, ib9m26iuq, ib9m30n2q, ib9m31trq, ib9m37giq, ib9m38c9q, ib9m42x3q, ib9m43xeq, ib9m48toq, ib9m52kqq, ib9m53l0q, ib9m57vdq, ib9m58irq, ib9m63whq, ib9m68thq, ib9m72unq, ib9m75hqq, ib9m80fgq, ib9m85d3q, ib9m89t9q, ib9m90tgq, ib9m95arq

12338 (18)	ibm901gqq, ibm902x6q, ibm903nxq, ibm904drq, ibm905nnq, ibm906lvq, ibm907jrq, ibm908nfq, ibm909n9q, ibm910heq, ibm911kbq, ibm912v7q, ibm913fzq, ibm919i1q, ibm920xfq, ibm921leq, ibm922exq, ibm923nyq, ibm924m6q, ibm925c5q, ibm926mzq, ibm927mdq, ibm928gwq, ibm929llq, ibm930z6q, ibm931fhq, ibm937irq, ibm938y5q, ibm939lmq, ibm940k0q, ibm941nfq, ibm942lnq, ibm943j2q, ibm944k0q, ibm945mtq, ibm946h4q, ibm947ltq, ibm948zuq, ibm949fnq
12712 (19)	ibvf01zpq, ibvf02s6q, ibvf03uiq, ibvf04utq, ibvf05b9q, ibvf06rmq, ibvf07eeq, ibvf13zxq, ibvf14sgq, ibvf15voq, ibvf16xeq, ibvf17btq, ibvf18t7q, ibvf19erq, ibvf25zcq, ibvf26ssq, ibvf27teq, ibvf28noq, ibvf29dyq, ibvf30btq
13098 (20)	ic4201mlq, ic4202usq, ic4203h6q, ic4204yqq, ic4205fuq, ic4206n4q, ic4207huq, ic4213kuq, ic4214knq, ic4215ihq, ic4216z1q, ic4217g4q, ic4218ndq, ic4219guq, ic4225lzq, ic4226quq, ic4227mqq, ic4228zmq, ic4229gcq, ic4230nqq
13587 (21)	icg901c9q, icg902wjq, icg903cyq, icg914pjq, icg915quq, icg916xcq, icg917dqq, icg918jkq, icg919k1q
14029 (22)	icql02rvq, icql03v7q, icql14esq, icql15o1q, icql16poq, icql17lwq, icql18rqq, icql19mrq
14391 (23)	id1n02v7q, id1n03ltq, id1n14t6q, id1n15ukq, id1n16utq, id1n17bfq, id1n18cuq, id1n19e6q
14548 (24)	idcl01hlq, idcl02myq, idcl13a1q, idcl14f9q, idcl15cxq, idcl16yeq, idcl17brq, idcl18cnq
14998 (25)	idpp01dkq, idpp02jeq, idpp13ayq, idpp14igq, idpp15kaq, idpp16g0q, idpp17jiq, idpp18rfq

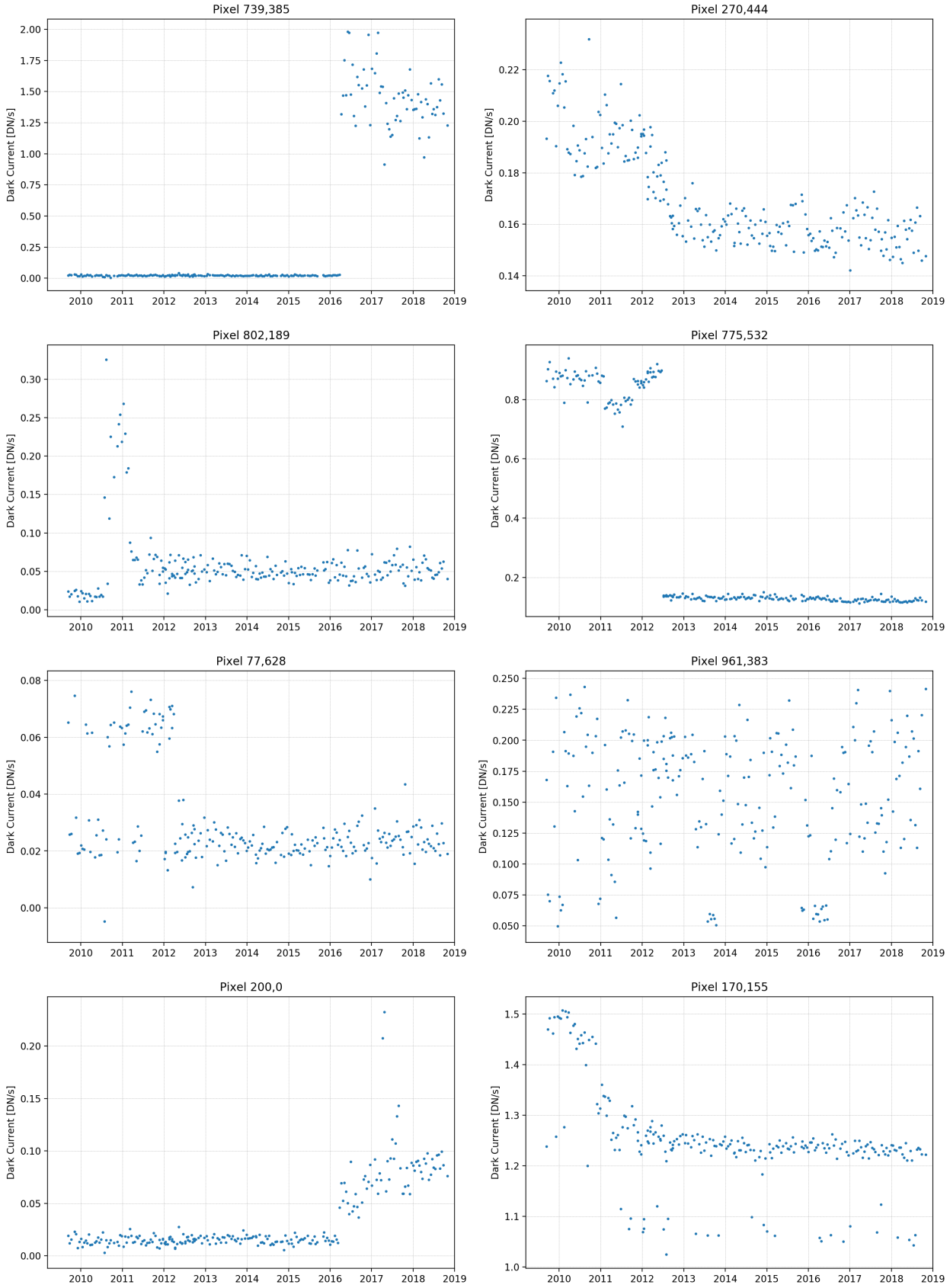

Figure 20: Examples of the behavior changes exhibited by WFC3/IR pixels.